Cosmography of anisotropic Kaniadakis holographic dark energy model in Brans-Dicke-Rastall gravity

Y. Aditya[1,a], D. Ram Babu[1,b], U.Y. Divya Prasanthi[2,c]
[1]Department of Mathematics, GMR Institute of Technology, Rajam-532127, India
[2]Department of Statistics & Mathematics, College of Horticulture, Dr. Y.S.R. Horticultural University, Parvathipuram-535502, India
[a]aditya.y@gmrit.edu.in; [b]rambabuphd23@gmail.com; [c]divyaaug24@gmail.com
(Submitted on 02.01.2025; Accepted on 07.03.2025)

Abstract. This study examines Kaniadakis holographic dark energy in the anisotropic and spatially homogeneous Bianchi type-II spacetime, framed within the Brans-Dicke-Rastall theory of gravity. The dark energy model is established by analyzing the correlation between the metric potentials to resolve the model's field equations. This results in a variable deceleration parameter that signifies a shift in the cosmic acceleration rate from deceleration to acceleration. This scenario involves the formulation of numerous cosmological parameters, including the scalar field, equation of state, deceleration, skewness, squared speed of sound, and statefinder parameters. The examination of these characteristics is presented through graphical representation. The examination of the evolution parameter substantiates the notion of holographic dark energy. Furthermore, the statefinder cosmic plane is linked to the $\lambda_{Ras}CDM$ framework and other recognized dark energy hypotheses.
Key words: Brans-Dicke-Rastall gravity, Bianchi type-II model, Kaniadakis holographic dark energy, Anisotropic model, Cosmology.

1 Introduction

A significant advancement in cosmology is the identification of the Universe's accelerated expansion, attributed to enigmatic dark energy (DE) (Perlmutter et al. 1999; Reiss et al. 1998; Spergel et al. 2007; Copeland et al. 2006). The nature and composition of DE remain open questions. Thermodynamic studies suggest that DE may consist of massless particles (bosons or fermions) behaving like a radiation fluid with negative pressure. The cosmological community widely accepts that DE acts as a repulsive force, akin to antigravity, responsible for the Universe's accelerated expansion. The Wilkinson Microwave Anisotropy Probe (WMAP) satellite experiment indicates that 73% of the Universe's composition is DE, 23% is non-baryonic dark matter, and the remaining 4% consists of ordinary baryonic matter and radiation. To comprehend DE, numerous dynamical models have been created, defined by the equation of state (EoS) parameter ω. The holographic DE (HDE) model, grounded on the holographic principle of quantum gravity (Susskind 1995), posits that the degrees of freedom in a confined system are finite and correlate with its boundary area rather than its volume. Cohen et al. (1999) determined that in a system characterized by an infrared cutoff scale L and an ultraviolet cutoff scale λ_{Ras}, the quantum vacuum energy must not exceed the mass of a black hole, expressed as $L^3\rho_{de} \lessapprox LM_p^2$, where ρ_{de} denotes the vacuum energy density and $M_p = (8\pi G)^{-1/2}$ represents the reduced Planck mass. Various entropy formalisms have been employed to develop and examine cosmological models. Recent HDE models comprise Tsallis HDE (THDE), Sharma-Mittal HDE (SMHDE), and Renyi HDE (RHDE) (Tavayef et al. 2018; Tsallis and Cirto 2013; Jahromi et al. 2018; Moradpour et al. 2018). Kaniadakis statistics, a generalized entropy measure (Kaniadakis 2001; Masi 2005; Abreu et al.

2018), have been utilized to investigate diverse gravitational and cosmological ramifications. The generalized δ-entropy (Kaniadakis), which signifies the entropy of a black hole, can be ascertained utilizing a solitary free parameter (Moradpour et al. 2020)

$$S_\delta = \frac{1}{\delta}\sinh(\delta S_{BH}), \tag{1}$$

where δ is an unknown parameter. The RHDE model, which assumes no interaction between cosmic sectors, shows greater stability (Moradpour et al. 2018). Discussions of SMHDE, THDE, and RHDE cosmological models in various contexts include Chern-Simons theory of gravity and the DGP braneworld (Younas et al. 2019, Maity and Debnath 2019, Iqbal and Jawad 2019). Observational constraints on RHDE and THDE models have been investigated by Prasanthi and Aditya (2021), Prasanthi and Aditya (2020), Aditya et al. (2019a), and Bhattacharjee (2020). Sharma and Dubey (2022) examined RHDE in a flat isotropic universe. The RHDE model with the particle and future horizons as the IR cutoff has been studied by Chunlen and Rangdee (2021). Santhi and Chinnappalanaidu (2022) investigated RHDE in Ruban's universe. Aditya and Prasanthi (2023), Aditya (2024) and Aditya et al. (2024) have studied SMHDE and RHDE models in modified theories of gravitation. Thus, by incorporating the concept of entropy and the notion of HDE, a novel model of DE called Kaniadakis HDE (KHDE) is proposed (Moradpour et al. 2020), which exhibits significant characteristics. Jawad and Sultan (2021), Sharma (2022) and Drepanou et al. (2022) have examined KHDE models within various gravitational theories. The dynamic structures of HDE, investigated by Sadeghi et al. (2022), have been analyzed within the context of Brans-Dicke's theory of gravity using the Tsallis and Kaniadakis approaches. Rao et al. (2024) have studied the anisotropic KHDE model in general relativity.

Another approach to understanding the Universe's accelerated expansion is modifying Einstein-Hilbert's action of general relativity (GR), leading to modified gravity theories. Among these, the study of Brans-Dicke (BD) (1961), Saez-Ballester (1986), $f(R)$ and $f(R,T)$ theories (Nojiri and Odintsov 2003; Capozziello and De Laurentis 2011; Harko et al. 2011) (where R is the curvature scalar and T is the trace of the energy-momentum tensor), and Brans-Dicke-Rastall (BDR) theory (Carames et al. 2014) are significant for explaining DE models.

Rastall Theory: Since the inception of GR, various geometric theories have been developed to explain gravitational phenomena (Brans and Dicke 1961; Rastall (1972, 1976); Moffat 1995; Bekenstein 2004). The conservation law is a critical aspect of GR. The pioneer non-conservative theory of gravity is the steady-state model (Bondi and Gold 1948; Hoyle 1948). In his non-conservative gravity theory, Rastall modified the conservation law $T^{ij}{}_{;i} = kR^{;j}$, where T is the energy-momentum tensor and R is the Ricci scalar curvature. This change shows that particle production in cosmology violates conventional conservation rules and may cause curvature. Rastall's Einstein equation modification is:

$$R_{ij} - \frac{1}{2}g_{ij}R = 8\pi G\left(T_{ij} - \frac{\lambda_{Ras}-1}{2}g_{ij}T\right)$$

$$T^{ij}_{;i} = \frac{\lambda_{Ras} - 1}{2} T^{;j}$$

where λ_{Ras} is Rastall's parameter, and setting $\lambda_{Ras} = 1$ recovers GR.
Brans-Dicke-Rastall Theory: In the BD context, identifying $G = \frac{1}{\phi}$, we have:

$$T^{ij}_{;i} = \frac{(1 - \lambda_{Ras})\phi}{16\pi} R^{;j}.$$

Generalizing Rastall's field equations to the BD case:

$$R_{ij} - \frac{\lambda_{Ras}}{2} g_{ij} R = \frac{8\pi}{\phi} T_{ij} + \frac{w}{\phi^2}\left(\phi_{;i}\phi_{;j} - \frac{1}{2} g_{ij}\phi_{;k}\phi^{;k}\right) + \frac{1}{\phi}\left(\phi_{;i;j} - g_{ij}\Box\phi\right)$$

in which the dimensionless BD parameter is denoted by w and the BD scalar field is denoted by ϕ. With these equations, we can find the trace:

$$R = \frac{1}{1 - 2\lambda_{Ras}}\left(\frac{8\pi}{\phi} T - \frac{w}{\phi^2}\phi_{;k}\phi^{;k} - 3\frac{\Box\phi}{\phi}\right).$$

Using this, the field equations become:

$$R_{ij} - \frac{1}{2} g_{ij} R = \frac{8\pi}{\phi}\left(T_{ij} - \frac{1 - \lambda_{Ras}}{2(1 - 2\lambda_{Ras})} g_{ij} T\right) + \frac{w}{\phi^2}\left(\phi_{;i}\phi_{;j} + \frac{\lambda_{Ras}}{2(1 - 2\lambda_{Ras})} g_{ij}\phi_{;k}\phi^{;k}\right) + \frac{1}{\phi}\left(\phi_{;i;j} + \frac{1 + \lambda_{Ras}}{2(1 - 2\lambda_{Ras})} g_{ij}\Box\phi\right). \quad (2)$$

The Bianchi identities lead to:

$$\Box\phi = \frac{8\pi\lambda_{Ras}}{3\lambda_{Ras} - 2(1 - 2\lambda_{Ras})w} T - \frac{w(1 - \lambda_{Ras})}{3\lambda_{Ras} - 2(1 - 2\lambda_{Ras})w} \frac{\phi^{;k}\phi_{;k}}{\phi}.$$

For $\lambda_{Ras} = 1$, the usual BD theory is recovered. The Kaluza-Klein modified holographic Ricci DE models in the BD theory of gravity have been reviewed by Aditya and Reddy (2018a). In their discussion of FLRW model within the context of the generalized Rastall theory of gravity, Das et al. (2018) utilized a perfect fluid as the matter source. Static self-gravitating systems are studied by Maurya and Ortiz (2020) within the context of Rastall gravity, with the aim of deducing star interiors. A comparison investigation of Einstein and Rastall's theories of gravity has been conducted by Darabi et al. (2018). The observational limitations on Rastall's cosmology have been investigated by Tang et al. (2019). In Rastall's theory of gravity, the flat FRW HDE model has been examined by Ghaffari et al. (2020). Anisotropic DE models in BDR theory have been researched by Salako and Jawad (2015), and FLRW metric has been examined by Salako et al. (2016). The static spherically symmetric model in Rastall gravity has been studied by Moradpour (2016), whereas the flat FRW model has been studied by Moradpour and Salako (2016). Researchers Bamba

et al. (2018) have examined Rastall gravity's thermodynamics under entropy adjustments. In Rastall gravity, Darabi et al. (2018) have addressed the topic of Einstein's static solution stability. In their work, Shabani and Ziaie (2020) established a relationship between Rastall-type and $f(R,T)$ gravities. The Rastall gravity extension of the conventional λ_{Ras}CDM model has been thoroughly examined by Akarsu et al. (2020). The authors Lin and Qian (2020) put forward a model of cosmic evolution within the framework of generalized Rastall gravity. Within the framework of Rastall's theory of gravity, Shamir et al. (2021) have investigated a number of solutions that are exactly cylindrically symmetric.

In order to comprehend the behavior of the Universe on a grand scale, spatio-homogeneous and anisotropic cosmological models are necessary. Extensive research has been conducted using GR to study these models in order to obtain an accurate picture of the early Universe. Physicists are highly interested in models such as BTs II, III, V, VI_0, VIII, and IX that describe anisotropic space-times, even though the Bianchi type (BT)-I Universe is the main contender for studying how anisotropy in the early Universe impacted present-day observations. A number of writers have investigated BT cosmological models within revised theories of gravity (Pradhan and Amirhashchi 2011; Adhav et al. 2011; Rao et al. 2015; Mishra and Sahoo 2014). The BT-II metric is significant in cosmology and theoretical physics due to its ability to describe a specific class of anisotropic, homogeneous models of the universe. Unlike the standard FLRW metric, which assumes a perfectly isotropic and homogeneous universe, the BT-II metric allows for directional dependence, meaning that different directions in space can expand or contract at different rates. This makes it suitable for modeling the early universe, where perfect isotropy might not hold. BT-II models, being anisotropic, offer a natural framework for investigating such early-universe conditions and studying how the universe might have transitioned to its current, mostly isotropic state. The BT-II metric plays a crucial role in exploring the possibilities of an anisotropic early universe, testing modified gravity theories, and addressing open questions in cosmology. The BT-II metric, when studied in the context of KHDE within the BDR theory of gravity, holds importance for several reasons related to cosmological modeling and understanding the evolution of the universe.

From the above discussion, it is evident that several researchers have examined anisotropic KHDE models of the universe. However, BT-II KHDE models within the context of BDR theory of gravity have not yet been studied in the literature. Motivated by this gap and the previous investigations, we examine the BT-II space-time filled with anisotropic KHDE in the BDR theory of gravity. This paper is organized as follows: In Section 2, we find the solutions to the field equations that reflect the KHDE model. In Section 3, we will go over the model's physical features. Section 4 presents an overview of the results and conclusions.

2 Metric and field equations

We consider the BT-II space-time in the form

$$ds^2 = -dt^2 + R^2dx^2 + S^2dy^2 + 2S^2xdydz + (S^2x^2 + R^2)dz^2 \tag{3}$$

where the parameters R and S are just functions of cosmic time t. The volume V of the BT-II space-time and the average scale factor $a(t)$ are defined as

$$V = [a(t)]^3 = R^2 S \tag{4}$$

The deceleration parameter q is given by

$$q = -1 - \frac{\dot{H}}{H^2}. \tag{5}$$

In this case, a dot above the line represents differentiation relative to cosmic time t. The source's energy-momentum tensor T_{ij}, which is anisotropic along several spatial directions, takes the following form:

$$\begin{aligned} T_{ij} &= diag[-p_x, -p_y, -p_z, \rho] \\ &= diag[-\omega_x, -\omega_y, -\omega_z, 1]\rho \end{aligned} \tag{6}$$

where the entire energy density and pressure in different directions of the Universe are represented by ρ and p_i, respectively. Here, the EoS parameters for each direction are denoted by ω_i and the relation between the energy density and the pressure of the universe is $p_i = \omega_i \rho$. The symbols $i = x, y, z$ represent the coordinates x, y, and z, correspondingly. Since matter has a pressure of zero and DE has a pressure that varies in all directions, we will assume in this article that DE and matter make up the Universe. This leads us to the following expression for the energy-momentum tensor:

$$\begin{aligned} T^m_{ij} &= diag[0, 0, 0, 1]\rho_m \\ T^{de}_{ij} &= diag[-\omega_{de}, -(\omega_{de} + \gamma), -\omega_{de}, 1]\rho_{de} \end{aligned} \tag{7}$$

which are the energy-momentum tensors of matter (T^m_{ij}) and DE (T^{de}_{ij}). So that things are easier to understand, let us assume that $\omega_x = \omega_y = \omega_z = \omega_{de}$ and that the skewness parameter γ is the y-direction divergence from the EoS parameter ω_{de}. The energy densities of matter are denoted as ρ_m and DE as ρ_{de} in this equation.

The BDR field equations (2) for the metric (3) in a comoving coordinate system can be formally expressed using (7) as

$$\begin{aligned} \frac{\ddot{S}}{S} + \frac{\ddot{R}}{R} + \frac{\dot{R}\dot{S}}{RS} + \frac{1}{4}\frac{S^2}{R^4} = \frac{8\pi}{\phi}\Bigg(&\frac{1+\lambda_{Ras}}{2-4\lambda_{Ras}}\omega_{de}\rho_{de} + \frac{1-\lambda_{Ras}}{2-4\lambda_{Ras}}\gamma\rho_{de} - \frac{1-\lambda_{Ras}}{2-4\lambda_{Ras}}(\rho_m + \rho_{de})\Bigg) \\ &+ w\left(\frac{\dot{\phi}}{\phi}\right)^2\left(\frac{\lambda_{Ras}}{2-4\lambda_{Ras}}\right) + \left(\frac{2-\lambda_{Ras}}{1-2\lambda_{Ras}}\right)\frac{\dot{R}}{R}\frac{\dot{\phi}}{\phi} \\ &+ \left(\frac{1+\lambda_{Ras}}{2-4\lambda_{Ras}}\right)\frac{\dot{S}}{S}\frac{\dot{\phi}}{\phi} + \left(\frac{1+\lambda_{Ras}}{2-4\lambda_{Ras}}\right)\frac{\ddot{\phi}}{\phi} \end{aligned} \tag{8}$$

$$\begin{aligned} 2\frac{\ddot{R}}{R} + \left(\frac{\dot{R}}{R}\right)^2 - \frac{3}{4}\frac{S^2}{R^4} = \frac{8\pi}{\phi}\Bigg(&\frac{1+\lambda_{Ras}}{2-4\lambda_{Ras}}\omega_{de}\rho_{de} + \frac{3\lambda_{Ras}-1}{2-4\lambda_{Ras}}\gamma\rho_{de} - \frac{1-\lambda_{Ras}}{2-4\lambda_{Ras}}(\rho_m + \rho_{de})\Bigg) \\ &+ w\left(\frac{\dot{\phi}}{\phi}\right)^2\left(\frac{\lambda_{Ras}}{2-4\lambda_{Ras}}\right) + \left(\frac{1+\lambda_{Ras}}{1-2\lambda_{Ras}}\right)\frac{\dot{R}}{R}\frac{\dot{\phi}}{\phi} \\ &+ \left(\frac{3-3\lambda_{Ras}}{2-4\lambda_{Ras}}\right)\frac{\dot{S}}{S}\frac{\dot{\phi}}{\phi} + \left(\frac{1+\lambda_{Ras}}{2-4\lambda_{Ras}}\right)\frac{\ddot{\phi}}{\phi} \end{aligned} \tag{9}$$

$$2\frac{\dot{R}}{R}\frac{\dot{S}}{S}+\left(\frac{\dot{R}}{R}\right)^2-\frac{1}{4}\frac{S^2}{R^4}=\frac{8\pi}{\phi}\left(\frac{1-3\lambda_{Ras}}{2-4\lambda_{Ras}}(\rho_m+\rho_{de})+\frac{3-3\lambda_{Ras}}{2-4\lambda_{Ras}}\omega_{de}\rho_{de}+\frac{1-\lambda_{Ras}}{2-4\lambda_{Ras}}\gamma\rho_{de}\right)$$
$$+w\left(\frac{\dot{\phi}}{\phi}\right)^2\left(\frac{2-3\lambda_{Ras}}{2-4\lambda_{Ras}}\right)+\left(\frac{1+\lambda_{Ras}}{1-2\lambda_{Ras}}\right)\frac{\dot{R}}{R}\frac{\dot{\phi}}{\phi}$$
$$+\left(\frac{1+\lambda_{Ras}}{2-4\lambda_{Ras}}\right)\frac{\dot{S}}{S}\frac{\dot{\phi}}{\phi}+\left(\frac{3-3\lambda_{Ras}}{2-4\lambda_{Ras}}\right)\frac{\ddot{\phi}}{\phi} \tag{10}$$

$$\ddot{\phi}+\left(\frac{2\dot{R}}{R}+\frac{\dot{S}}{S}\right)\dot{\phi}=\left(\frac{8\pi\lambda_{Ras}(\rho_{de}+\rho_m-3\omega_{de}\rho_{de}-\gamma\rho_{de})}{3\lambda_{Ras}-2(1-2\lambda_{Ras})w}\right)$$
$$-\left(\frac{w(1-\lambda_{Ras})}{3\lambda_{Ras}-2(1-2\lambda_{Ras})w}\right)\left(\frac{\dot{\phi}^2}{\phi}\right). \tag{11}$$

The field equations, as shown in Eqs. (8) to (11), are a set of four separate equations with a total of six unknowns, including R, S, ρ_{de}, ω_{de}, ρ_m, and γ. We have to solve them if we want a deterministic answer. Assuming the following physically reasonable condition can help with this:

- The model's expansion scalar $\theta=\frac{2\dot{R}}{R}+\frac{\dot{S}}{S}$ is directly related to the shear scalar $\sigma^2=\frac{1}{3}\left(\frac{\dot{R}}{R}-\frac{\dot{S}}{S}\right)^2$ of the model, creating a relationship between the metric potentials as $R=S^n$, where $n\neq 1$ is an arbitrary constant. Thorne (1967) gives a detailed account of this connection and the importance of it. Evidence from observations points to the fact that the universe's Hubble expansion is currently isotropic within around ±30% Kristian and Sachs (1966), Kantowski and Sachs (1966), and observations at redshift limit this range to $\frac{\sigma}{H}\leq 0.3$. The normal congruence, where $\frac{\sigma}{H}$ remains constant, is derived from the work of Collins et al. (1980) and holds for a spatially homogeneous space-time.
- The following power-law relationship is often used in literature: $\phi\propto[a(t)]^k$, where k is a power index, and it is used to describe the relationship between the scalar field ϕ and the average scale factor $a(t)$ (Johri and Sudharsan 1989 ; Johri and Desikan 1994). Researchers (Santhi et al. 2016a; Santhi et al. 2017a; Aditya et al. 2020; Aditya et al. 2019b) explored different aspects of this scalar field ϕ. We simplify the mathematical complexity of the system by making the following assumption, given the physical significance of this relationship:
$$\phi(t)=\phi_0[a(t)]^k \tag{12}$$
where ϕ_0 is a proportionality constant.

Using the above relations in Eqs. (9) and (10), we get

$$\frac{\ddot{S}}{S}+\left(\frac{6n+2kn+k}{3}\right)\frac{\dot{S}}{S}=\frac{1}{n-1}\frac{S^{3-4n}}{\dot{S}}-\frac{1}{n-1}\frac{8\pi\gamma}{\phi}\frac{S}{\dot{S}}\rho_{de}. \tag{13}$$

The relationship between DE's energy density and the skewness or deviation parameter has been the subject of numerous recent investigations. Anisotropic DE models were investigated by Akarsu and Kilinc (2010), who took into

account a correlation between DE energy density and skewness factors. In a similar vein, Sharif and Zubair (2010) examined dynamical anisotropic DE models using the identical relation. We presuppose the following relationship between $\gamma(t)$ and ρ_{de} in order to completely resolve Eq. (13)

$$\gamma(t) = \frac{\phi}{8\pi\rho_{de}}\left[S^{2-4n} - (n-1)\gamma_0\frac{\dot{S}}{S}\right] \tag{14}$$

in which every given constant is represented by γ_0. Various authors have explored comparable relationships in the literature (Adhav 2011; Santhi et al. 2016b). One example is the use of the same relation to assess anisotropic DE models by Santhi et al. (2017b) and Aditya and Reddy (2018b). We can find our model's metric potentials by plugging the Eq. (14) into Eq. (13)

$$S = \left(k_1 e^{\gamma_0 t} + k_2\right)^{\frac{b_2}{k_2}}, \qquad R = \left(k_1 e^{\gamma_0 t} + k_2\right)^{\frac{nb_2}{k_2}} \tag{15}$$

where $k_1 = \frac{(2n+1)(k+3)}{3}\frac{b_1}{\gamma_0}$, $k_2 = \frac{(2n+1)(k+3)b_2}{3}$, b_1 and b_2 are integrating constants. Now using these metric potentials (15), we can rewrite the space-time as

$$\begin{aligned} ds^2 = &-dt^2 + \left(k_1 e^{\gamma_0 t} + k_2\right)^{\frac{2nb_2}{k_2}} dx^2 + \left(k_1 e^{\gamma_0 t} + k_2\right)^{\frac{2b_2}{k_2}} dy^2 \\ &+2\left(k_1 e^{\gamma_0 t} + k_2\right)^{\frac{2b_2}{k_2}} xdydz \\ &+\left(\left(k_1 e^{\gamma_0 t} + k_2\right)^{\frac{2b_2}{k_2}} x^2 + \left(k_1 e^{\gamma_0 t} + k_2\right)^{\frac{2nb_2}{k_2}}\right) dz^2. \end{aligned} \tag{16}$$

Now from Eq. (12), the scalar field ϕ calculated as

$$\phi = \phi_0\left(k_1 e^{\gamma_0 t} + k_2\right)^{\frac{b_2 k(2n+1)}{3k_2}}. \tag{17}$$

The mean Hubble parameter H can be obtained as

$$H = \frac{(2n+1)b_2 k_1 \gamma_0 e^{\gamma_0 t}}{3k_2\left(k_1 e^{\gamma_0 t} + k_2\right)} \tag{18}$$

KHDE: According to the HDE, if the present accelerated expansion of the Universe is caused by DE, then, according to the Kaniadakis black hole entropy shown in Eq. (1), the energy of a vacuum within a box of size L^3 shouldn't be higher than that of a black hole of the same size. As a result, this expression is

$$\lambda_{Ras}^4 \equiv \rho_{DE} \propto \frac{\mathcal{S}_\delta}{\mathcal{L}^4} \tag{19}$$

as ρ_{DE}, the vacuum energy. Since the infrared cutoff is defined by the Hubble horizon of the universe, we can deduce that $A = \frac{4\pi}{H^2}$,

$$\rho_{DE} = \frac{3d^2H^4}{\delta} sinh\left(\frac{\pi\delta}{H^2}\right) \tag{20}$$

The value of the constant d^2 is not known in the given statement, δ belongs to the set of real numbers, and the Hubble parameter is represented by $H = \frac{\dot{a}}{a}$. The convergence of ρ_{kde} to $\frac{3d^2H^4}{\delta}$ is obvious as $k \to 0$, and this corresponds to the well-established Bekenstein entropy-based HDE. A DE candidate with a pressure p_{kde} and a density ρ_{kde} is being considered in this scenario, along with a pressure-less fluid with an energy density ρ_m. Eq. (20), with the help of equations (15) and (17), yields the KHDE energy density as

$$\rho_{de} = \frac{c^2\left(2\,n+1\right)^4 {b_2}^4 {k_1}^4 {\gamma_0}^4 \left(e^{\gamma_0 t}\right)^4}{27{k_2}^4\left(k_1 e^{\gamma_0 t}+k_2\right)^4 \kappa} \sinh\left(\frac{9\pi\,\kappa\,{k_2}^2\left(k_1 e^{\gamma_0 t}+k_2\right)^2}{\left(2\,n+1\right)^2 {b_2}^2 {k_1}^2 {\gamma_0}^2 \left(e^{\gamma_0 t}\right)^2}\right) \tag{21}$$

The BT-II universe with KHDE inside the framework of BDR theory of gravity is shown by Eq. (16), the scalar field (17), and the energy density (21). The energy density of matter is calculated as

$$\begin{aligned}
\rho_m \;=\; & \left(\frac{3-3\,\lambda_{Ras}}{2-4\,\lambda_{Ras}}\left(\frac{\phi_0}{8\pi}\left(k_1 e^{\gamma_0 t}+k_2\right)^{\frac{b_2 k\left(2\,n+1\right)}{3k_2}}\left(\frac{{b_2}^2{k_1}^2{\gamma_0}^2\left(e^{\gamma_0 t}\right)^2+{k_2}^2 b_2 k_1{\gamma_0}^2 e^{\gamma_0 t}}{{k_2}^2\left(k_1 e^{\gamma_0 t}+k_2\right)^2}\right.\right.\right.\\
& +\frac{n^2{b_2}^2{k_1}^2{\gamma_0}^2\left(e^{\gamma_0 t}\right)^2+{k_2}^2 n b_2 k_1{\gamma_0}^2 e^{\gamma_0 t}}{{k_2}^2\left(k_1 e^{\gamma_0 t}+k_2\right)^2}+\frac{n{b_2}^2{k_1}^2{\gamma_0}^2\left(e^{\gamma_0 t}\right)^2}{{k_2}^2\left(k_1 e^{\gamma_0 t}+k_2\right)^2}\\
& +\frac{1}{4}\left(\left(k_1 e^{\gamma_0 t}+k_2\right)^{\frac{b_2}{k_2}}\right)^2\left(\left(k_1 e^{\gamma_0 t}+k_2\right)^{\frac{nb_2}{k_2}}\right)^{-4}-\frac{w{b_2}^2k^2\left(2\,n+1\right)^2{k_1}^2{\gamma_0}^2\left(e^{\gamma_0 t}\right)^2\lambda_{Ras}}{9{k_2}^2\left(k_1 e^{\gamma_0 t}+k_2\right)^2\left(2-4\,\lambda_{Ras}\right)}\\
& -\frac{\left(2-\lambda_{Ras}\right)n{b_2}^2{k_1}^2{\gamma_0}^2\left(e^{\gamma_0 t}\right)^2 k\left(2\,n+1\right)}{3\left(1-2\,\lambda_{Ras}\right){k_2}^2\left(k_1 e^{\gamma_0 t}+k_2\right)^2}-\frac{\left(1+\lambda_{Ras}\right){b_2}^2{k_1}^2{\gamma_0}^2\left(e^{\gamma_0 t}\right)^2 k\left(2\,n+1\right)}{3{k_2}^2\left(k_1 e^{\gamma_0 t}+k_2\right)^2\left(2-4\,\lambda_{Ras}\right)}\\
& \left.\left.-\frac{\left(1+\lambda_{Ras}\right)\left({b_2}^2k^2\left(2\,n+1\right)^2{k_1}^2{\gamma_0}^2\left(e^{\gamma_0 t}\right)^2+3\,{k_2}^2 b_2 k\left(2\,n+1\right)k_1{\gamma_0}^2 e^{\gamma_0 t}\right)}{9{k_2}^2\left(k_1 e^{\gamma_0 t}+k_2\right)^2\left(2-4\,\lambda_{Ras}\right)}\right)\right.\\
& +\frac{\left(\lambda_{Ras}-1\right)\phi_0}{8\left(2-4\,\lambda_{Ras}\right)\pi}\left(k_1 e^{\gamma_0 t}+k_2\right)^{\frac{b_2 k\left(2\,n+1\right)}{3k_2}}\left(\left(\left(k_1 e^{\gamma_0 t}+k_2\right)^{\frac{b_2}{k_2}}\right)^{2-4\,n}-\frac{\left(n-1\right){\gamma_0}^2 b_2 k_1 e^{\gamma_0 t}}{k_2\left(k_1 e^{\gamma_0 t}+k_2\right)}\right)\Bigg)\\
& -\frac{1+\lambda_{Ras}}{2-4\,\lambda_{Ras}}\left(\frac{\phi_0}{8\pi}\left(k_1 e^{\gamma_0 t}+k_2\right)^{\frac{b_2 k\left(2\,n+1\right)}{3k_2}}\left(\frac{2n{b_2}^2{k_1}^2{\gamma_0}^2\left(e^{\gamma_0 t}\right)^2}{{k_2}^2\left(k_1 e^{\gamma_0 t}+k_2\right)^2}+\frac{n^2{b_2}^2{k_1}^2{\gamma_0}^2\left(e^{\gamma_0 t}\right)^2}{{k_2}^2\left(k_1 e^{\gamma_0 t}+k_2\right)^2}\right.\right.\\
& -\frac{1}{4}\left(\left(k_1 e^{\gamma_0 t}+k_2\right)^{\frac{b_2}{k_2}}\right)^2\left(\left(k_1 e^{\gamma_0 t}+k_2\right)^{\frac{nb_2}{k_2}}\right)^{-4}-\frac{w{b_2}^2k^2\left(2\,n+1\right)^2{k_1}^2{\gamma_0}^2\left(e^{\gamma_0 t}\right)^2\left(2-3\,\lambda_{Ras}\right)}{9{k_2}^2\left(k_1 e^{\gamma_0 t}+k_2\right)^2\left(2-4\,\lambda_{Ras}\right)}\\
& -\frac{\left(1+\lambda_{Ras}\right)n{b_2}^2{k_1}^2{\gamma_0}^2\left(e^{\gamma_0 t}\right)^2 k\left(2\,n+1\right)}{3\left(1-2\,\lambda_{Ras}\right){k_2}^2\left(k_1 e^{\gamma_0 t}+k_2\right)^2}-\frac{\left(1+\lambda_{Ras}\right){b_2}^2{k_1}^2{\gamma_0}^2\left(e^{\gamma_0 t}\right)^2 k\left(2\,n+1\right)}{3{k_2}^2\left(k_1 e^{\gamma_0 t}+k_2\right)^2\left(2-4\,\lambda_{Ras}\right)}\\
& \left.\left.-\frac{\left(3-3\,\lambda_{Ras}\right)\left({b_2}^2k^2\left(2\,n+1\right)^2{k_1}^2{\gamma_0}^2\left(e^{\gamma_0 t}\right)^2+3\,{k_2}^2 b_2 k\left(2\,n+1\right)k_1{\gamma_0}^2 e^{\gamma_0 t}\right)}{9{k_2}^2\left(k_1 e^{\gamma_0 t}+k_2\right)^2\left(2-4\,\lambda_{Ras}\right)}\right)\right.\\
& +\frac{\left(\lambda_{Ras}-1\right)\phi_0}{8\left(2-4\,\lambda_{Ras}\right)\pi}\left(k_1 e^{\gamma_0 t}+k_2\right)^{\frac{b_2 k\left(2\,n+1\right)}{3k_2}}\left(\left(\left(k_1 e^{\gamma_0 t}+k_2\right)^{\frac{b_2}{k_2}}\right)^{2-4\,n}-\frac{\left(n-1\right){\gamma_0}^2 b_2 k_1 e^{\gamma_0 t}}{k_2\left(k_1 e^{\gamma_0 t}+k_2\right)}\right)\Bigg)\Bigg)\\
& \times\left(-\frac{\left(1+\lambda_{Ras}\right)\left(1-3\,\lambda_{Ras}\right)}{\left(2-4\,\lambda_{Ras}\right)^2}+\frac{\left(\lambda_{Ras}-1\right)\left(3-3\,\lambda_{Ras}\right)}{\left(2-4\,\lambda_{Ras}\right)^2}\right)^{-1}\\
& -\frac{c^2\left(2\,n+1\right)^4{b_2}^4{k_1}^4{\gamma_0}^4\left(e^{\gamma_0 t}\right)^4}{27{k_2}^4\left(k_1 e^{\gamma_0 t}+k_2\right)^4\kappa}\sinh\left(9\,\frac{\pi\,\kappa\,{k_2}^2\left(k_1 e^{\gamma_0 t}+k_2\right)^2}{\left(2\,n+1\right)^2{b_2}^2{k_1}^2{\gamma_0}^2\left(e^{\gamma_0 t}\right)^2}\right).
\end{aligned}$$

3 Cosmological parameters and discussion

Here we define some physical and geometrical factors that will be useful for studying the dynamics of our KHDE model within the context of BDR theory of gravity.

Scalar field Figure 1 illustrates the evolution of a scalar field with respect to cosmic time for different values of the parameter γ_0, which significantly influences its behavior over time. It is evident from the plot that the scalar field decreases as cosmic time progresses. Additionally, we observe that the scalar field's decrease is accompanied by an increase in its kinetic energy. This trend closely resembles the behavior observed in scalar field models of DE developed in existing literature (Jawad et al. 2015; Naidu et al. 2021; Aditya et al. 2021).

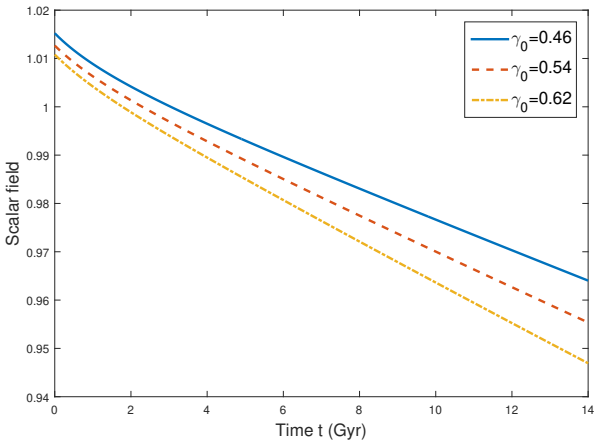

Fig. 1. Plot of scalar field versus cosmic time t for $k = -0.021$, $n = 0.97$, $b_1 = 4.1$, $b_2 = -1.12$ and $\phi_0 = 1.021$.

Energy Conditions We explore well-known energy conditions in our KHDE model. The Raychaudhuri equations, which are fundamental to any discussion of the consistency of null and time-like geodesics, are the starting point for the investigation of energy conditions. A number of broad theorems on the behavior of strong gravitational fields can be proven using these energy requirements as basic instruments. The following are the typical energy conditions:

- Null energy conditions (NEC) : $\rho_{de} + p_{de} \geq 0$,
- Strong energy conditions (SEC) : $\rho_{de} + p_{de} \geq 0$, $\rho_{de} + 3p_{de} \geq 0$,
- Weak energy conditions (WEC) : $\rho_{de} \geq 0$, $\rho_{de} + p_{de} \geq 0$,
- Dominant energy condition (DEC) : $\rho_{de} \geq 0$, $\rho_{de} \pm p_{de} \geq 0$.

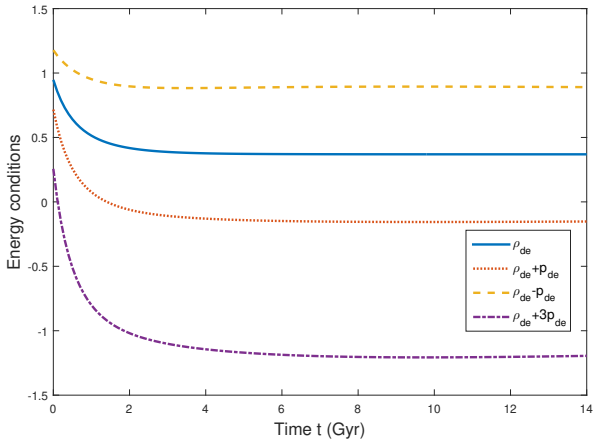

Fig. 2. Plot of energy conditions versus cosmic time t for $\gamma_0 = 0.54$, $k = -0.021$, $n = 0.97$, $b_1 = 4.1$, $b_2 = -1.12$, $\lambda_{Ras} = 70.28$, $\phi_0 = 1.021$, $w = 252$, $c = 0.85$ and $\kappa = 0.019$.

According to the NEC, the universe's energy density decreases with expansion, and the Big Rip phenomenon could happen if the NEC is violated. Conversely, the acceleration of cosmic expansion is signified by the SEC violation. The proof of the SEC and WEC is required by the Hawking-Penrose singularity theorems. Because violating the WEC or NEC might cause the violation of other energy conditions, they are of particular relevance among all energy conditions. Our KHDE model's energy conditions are shown in Figure 2. With $\rho_{de} \geq 0$, it is clear from the plot that the WEC is satisfied. But the SEC condition $\rho_{de} + 3p_{de} \geq 0$ is not satisfied. The present observable evidence is in agreement with the theory that this violation is due to the universe's accelerated expansion in its latter phases.

EoS Parameter The relationship between a fluid's pressure p and energy density ρ is described by the EoS parameter ω, which is defined as $\frac{p}{\rho}$. Various ω values represent different phases of the universe's expansion, from the early, slowing phases to the current, fast-growing ones.
For instance, during the early phases:
- Stiff fluid corresponds to $\omega = 1$,
- Radiation domination is characterized by $\omega = \frac{1}{3}$,
- Matter domination (dust) is represented by $\omega = 0$,

In later stages, during the accelerating expansion:
- Quintessence is indicated by $-1 < \omega < -1/3$,
- A cosmological constant corresponds to $\omega = -1$,
- Phantom energy is represented by $\omega < -1$.

From Eqs. (8), (9), (15), (17) and (21), we get the EoS parameter of our model as

$$
\begin{aligned}
\omega_{de} = {} & \frac{27{k_2}^4\left(k_1e^{\gamma_0 t}+k_2\right)^4\kappa}{c^2\left(2\,n+1\right)^4{b_2}^4{k_1}^4{\gamma_0}^4\left(e^{\gamma_0 t}\right)^4}\left(\frac{1-3\,\lambda_{Ras}}{2-4\,\lambda_{Ras}}\left(\frac{\phi_0}{8\pi}\left(k_1e^{\gamma_0 t}+k_2\right)^{\frac{b_2k(2\,n+1)}{3k_2}}\right.\right.\\
& \left(\frac{{b_2}^2{k_1}^2{\gamma_0}^2\left(e^{\gamma_0 t}\right)^2+{k_2}^2b_2k_1{\gamma_0}^2e^{\gamma_0 t}}{{k_2}^2\left(k_1e^{\gamma_0 t}+k_2\right)^2}+\frac{n^2{b_2}^2{k_1}^2{\gamma_0}^2\left(e^{\gamma_0 t}\right)^2+{k_2}^2nb_2k_1{\gamma_0}^2e^{\gamma_0 t}}{{k_2}^2\left(k_1e^{\gamma_0 t}+k_2\right)^2}\right.\\
& +\frac{nb_2{}^2{k_1}^2{\gamma_0}^2\left(e^{\gamma_0 t}\right)^2}{{k_2}^2\left(k_1e^{\gamma_0 t}+k_2\right)^2}+\frac{1}{4}\left(\left(k_1e^{\gamma_0 t}+k_2\right)^{\frac{b_2}{k_2}}\right)^2\left(\left(k_1e^{\gamma_0 t}+k_2\right)^{\frac{nb_2}{k_2}}\right)^{-4}\\
& -\frac{wb_2{}^2k^2\left(2\,n+1\right)^2{k_1}^2{\gamma_0}^2\left(e^{\gamma_0 t}\right)^2\lambda_{Ras}}{9{k_2}^2\left(k_1e^{\gamma_0 t}+k_2\right)^2\left(2-4\,\lambda_{Ras}\right)}-\frac{\left(2-\lambda_{Ras}\right)nb_2{}^2{k_1}^2{\gamma_0}^2\left(e^{\gamma_0 t}\right)^2k\left(2\,n+1\right)}{3\left(1-2\,\lambda_{Ras}\right){k_2}^2\left(k_1e^{\gamma_0 t}+k_2\right)^2}\\
& -\frac{\left(1+\lambda_{Ras}\right)\left({b_2}^2k^2\left(2\,n+1\right)^2{k_1}^2{\gamma_0}^2\left(e^{\gamma_0 t}\right)^2+3\,{k_2}^2b_2k\left(2\,n+1\right)k_1{\gamma_0}^2e^{\gamma_0 t}\right)}{9{k_2}^2\left(k_1e^{\gamma_0 t}+k_2\right)^2\left(2-4\,\lambda_{Ras}\right)}\\
& \left.-\frac{\left(1+\lambda_{Ras}\right)b_2{}^2{k_1}^2{\gamma_0}^2\left(e^{\gamma_0 t}\right)^2k\left(2\,n+1\right)}{3{k_2}^2\left(k_1e^{\gamma_0 t}+k_2\right)^2\left(2-4\,\lambda_{Ras}\right)}\right)+\frac{\left(\lambda_{Ras}-1\right)\phi_0}{8\left(2-4\,\lambda_{Ras}\right)\pi}\left(k_1e^{\gamma_0 t}+k_2\right)^{\frac{b_2k(2\,n+1)}{3k_2}}\\
& \left.\times\left(\left(\left(k_1e^{\gamma_0 t}+k_2\right)^{\frac{b_2}{k_2}}\right)^{2-4\,n}-\frac{\left(n-1\right){\gamma_0}^2b_2k_1e^{\gamma_0 t}}{k_2\left(k_1e^{\gamma_0 t}+k_2\right)}\right)\right)\\
& -\frac{\lambda_{Ras}-1}{2-4\,\lambda_{Ras}}\left(\frac{\phi_0}{8\pi}\left(k_1e^{\gamma_0 t}+k_2\right)^{\frac{b_2k(2\,n+1)}{3k_2}}\left(\frac{2nb_2{}^2{k_1}^2{\gamma_0}^2\left(e^{\gamma_0 t}\right)^2}{{k_2}^2\left(k_1e^{\gamma_0 t}+k_2\right)^2}+\frac{n^2{b_2}^2{k_1}^2{\gamma_0}^2\left(e^{\gamma_0 t}\right)^2}{{k_2}^2\left(k_1e^{\gamma_0 t}+k_2\right)^2}\right.\right.\\
& -\frac{1}{4}\left(\left(k_1e^{\gamma_0 t}+k_2\right)^{\frac{b_2}{k_2}}\right)^2\left(\left(k_1e^{\gamma_0 t}+k_2\right)^{\frac{nb_2}{k_2}}\right)^{-4}-\frac{wb_2{}^2k^2\left(2\,n+1\right)^2{k_1}^2{\gamma_0}^2\left(e^{\gamma_0 t}\right)^2\left(2-3\,\lambda_{Ras}\right)}{9{k_2}^2\left(k_1e^{\gamma_0 t}+k_2\right)^2\left(2-4\,\lambda_{Ras}\right)}\\
& -\frac{\left(1+\lambda_{Ras}\right)nb_2{}^2{k_1}^2{\gamma_0}^2\left(e^{\gamma_0 t}\right)^2k\left(2\,n+1\right)}{3\left(1-2\,\lambda_{Ras}\right){k_2}^2\left(k_1e^{\gamma_0 t}+k_2\right)^2}-\frac{\left(1+\lambda_{Ras}\right)b_2{}^2{k_1}^2{\gamma_0}^2\left(e^{\gamma_0 t}\right)^2k\left(2\,n+1\right)}{3{k_2}^2\left(k_1e^{\gamma_0 t}+k_2\right)^2\left(2-4\,\lambda_{Ras}\right)}\\
& \left.\left.-\frac{\left(3-3\,\lambda_{Ras}\right)\left({b_2}^2k^2\left(2\,n+1\right)^2{k_1}^2{\gamma_0}^2\left(e^{\gamma_0 t}\right)^2+3\,{k_2}^2b_2k\left(2\,n+1\right)k_1{\gamma_0}^2e^{\gamma_0 t}\right)}{9{k_2}^2\left(k_1e^{\gamma_0 t}+k_2\right)^2\left(2-4\,\lambda_{Ras}\right)}\right)\right.\\
& \left.+\frac{\left(\lambda_{Ras}-1\right)\phi_0}{8\left(2-4\,\lambda_{Ras}\right)\pi}\left(k_1e^{\gamma_0 t}+k_2\right)^{\frac{b_2k(2\,n+1)}{3k_2}}\left(\left(\left(k_1e^{\gamma_0 t}+k_2\right)^{\frac{b_2}{k_2}}\right)^{2-4\,n}-\frac{\left(n-1\right){\gamma_0}^2b_2k_1e^{\gamma_0 t}}{k_2\left(k_1e^{\gamma_0 t}+k_2\right)}\right)\right)\right)\\
& \times\left(\frac{\left(1+\lambda_{Ras}\right)\left(1-3\,\lambda_{Ras}\right)}{\left(2-4\,\lambda_{Ras}\right)^2}-\frac{\left(\lambda_{Ras}-1\right)\left(3-3\,\lambda_{Ras}\right)}{\left(2-4\,\lambda_{Ras}\right)^2}\right)^{-1}\left(\sinh\left(\frac{9\pi\,\kappa\,{k_2}^2\left(k_1e^{\gamma_0 t}+k_2\right)^2}{\left(2\,n+1\right)^2{b_2}^2{k_1}^2{\gamma_0}^2\left(e^{\gamma_0 t}\right)^2}\right)\right)^{-1}
\end{aligned}
$$

We can see how the EoS parameter for our KHDE model changes with different c values in Fig. 2. At first, the model starts in the quintessence epoch and moves on to the phantom epoch when it crosses the phantom dividing line ($\omega_{de} = -1$). Because of this quality, the universe acts in a quintom fashion. Higher phantom values are also the tendency of the model when parameter c decreases. Furthermore, according to recent Planck data, the present values of EoS parameter in our model agree with the data (Aghanim et al. 2020).

$\omega_{de} - \omega'_{de}$ plane Researching the dynamical characteristics of DE models can be greatly facilitated by the $\omega_{de} - \omega'_{de}$ plane analysis. Under these circumstances, prime ($\prime$) means differentiation with regard to $\ln a$, where a is the universe's scale factor. This approach, which was first suggested by Caldwell and Linder (2005), makes it easier to divide the $\omega_{de}-\omega'_{de}$ plane into parts where it is thawing and regions where it is freezing. In thawing regions, $\omega_{de} < 0$ and

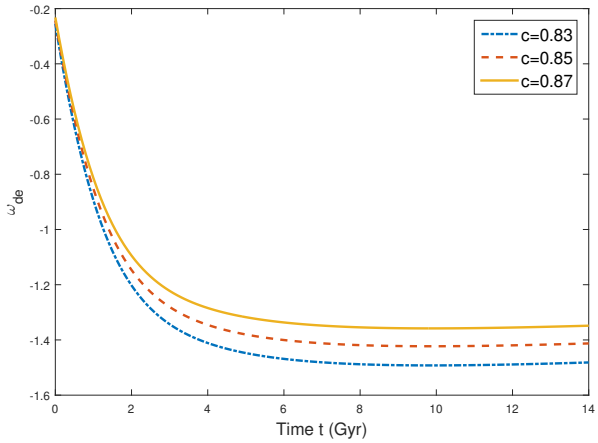

Fig. 3. Plot of EoS parameter versus cosmic time t for $\gamma_0 = 0.54$, $k = -0.021$, $n = 0.97$, $b_1 = 4.1$, $b_2 = -1.12$, $\lambda_{Ras} = 70.28$, $\phi_0 = 1.021$, $w = 252$ and $\kappa = 0.019$.

$\omega'_{de} > 0$ stand for the DE component, which is changing towards less negative values as the universe expands. On the other hand, freezing regions are indicated by $\omega_{de} < 0$ and $\omega'_{de} < 0$, which implies that the DE stays around the same or gets more negative as time goes on, even if the universe is expanding.

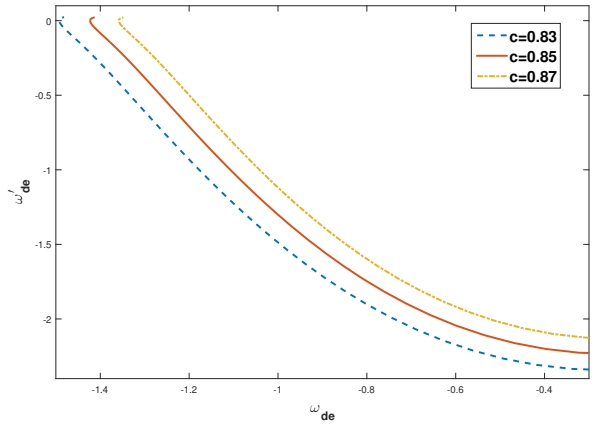

Fig. 4. Plot of $\omega_{de} - \omega'_{de}$ plane for $\gamma_0 = 0.54$, $k = -0.021$, $n = 0.97$, $b_1 = 4.1$, $b_2 = -1.12$, $\lambda_{Ras} = 70.28$, $\phi_0 = 1.021$, $w = 252$ and $\kappa = 0.019$.

We obtained the ω'_{de} of our model by differentiating Eq. (22) with respect to $\ln(a(t))$. Fig. 4 illustrates the $\omega_{de} - \omega'_{de}$ plane behavior for our KHDE model

across different values of parameter c. Initially, our model starts from the freezing region and transitions into the thawing region at the present epoch. However, it predominantly resides in the freezing region throughout its evolution. Modern cosmological observations suggest that the freezing region corresponds to a higher cosmic acceleration era compared to the thawing region. Therefore, our model's preference for the freezing region aligns well with observational evidence, indicating cosmic acceleration. Additionally, the present values of ω'_{de} from our model are consistent with contemporary Planck data (Ade et al. 2014 and Hinshaw 2018).

Stability analysis An essential quantity to evaluate in order to determine the KHDE model's stability is the squared speed of sound, abbreviated as v_s^2:

$$v_s^2 = \frac{\dot{p}_{de}}{\dot{\rho}_{de}} = \omega_{de} + \frac{\rho_{de}}{\dot{\rho}_{de}}\ \dot{\omega}_{de}. \tag{22}$$

Figure 5 shows the relationship between cosmic time (t) and v_s^2 for different values of c. The positive value of v_s^2 at the initial epoch and its continued negative value at present and late times may be seen clearly in Fig. 5. Therefore, our model is stable at the beginning of time but becomes unstable as time progresses. It is worth noting that similar findings of instability have been reported by several authors in the literature when studying stability analysis of DE models in various gravitational theories. Myung (2007) studied difference between HDE, Chaplygin gas, and tachyon model with constant potential. For this purpose, they examined squared speeds of sound and found that the squared speed for HDE is always negative and hence HDE is classically unstable. Similarly, Jawad et al. (2015) and Jawad and Chattopadhyay (2015) have discussed stability analysis of HDE models and found the unstable behavior of HDE models in their study.

Deceleration parameter The model's expansion is characterized by accelerating or decelerating depending on the deceleration parameter q. In particular, $q > 0$ denotes slowing down, $q = 0$ means keeping the expansion constant, and $-1 < q < 0$ means speeding up the growth. A super-exponential expansion is indicated by $q < -1$ while de Sitter (exponential) expansion is suggested by $q = -1$. Here is the formula for our model's deceleration parameter:

$$q = -1 - \frac{3{k_2}^2}{(2\,n+1)\,b_2 k_1 e^{\gamma_0 t}}. \tag{23}$$

The deceleration parameter's evolution relative to cosmic time for different values of γ_0 is shown in Fig. 6. It is worth mentioning that our model follows the observable universe's behavior as it smoothly moves from an early decelerated phase to its present accelerated phase.

Statefinder parameters The accelerated expansion of the cosmos has been explained by numerous DE theories in recent years. However, these models

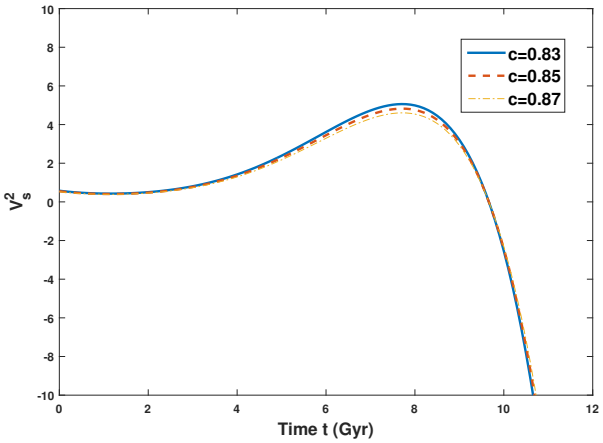

Fig. 5. Plot of v_s^2 versus cosmic time t for $\gamma_0 = 0.54$, $k = -0.021$, $n = 0.97$, $b_1 = 4.1$, $b_2 = -1.12$, $\lambda_{Ras} = 70.28$, $\phi_0 = 1.021$, $w = 252$ and $\kappa = 0.019$.

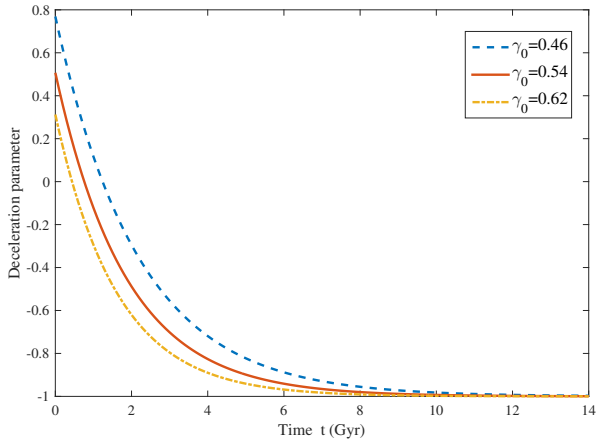

Fig. 6. Plot of deceleration parameter versus cosmic time t for $k = -0.021$, $n = 0.97$, $b_1 = 4.1$ and $b_2 = -1.12$.

often provide Hubble and deceleration parameters with identical present values, making differentiation difficult. To overcome this issue, Sahni et al. (2003) suggested combining deceleration and Hubble parameters, written as

$$r = \frac{\dddot{a}}{aH^3}, \quad s = \frac{r-1}{3(q-\frac{1}{2})}. \tag{24}$$

The regions shown below are defined by these statefinders: $\lambda_{Ras}CDM$ for $(r, s) = (1, 0)$ and CDM model for $(r, s) = (1, 1)$; $r < 1$ gives quintessence and

$s>0$ gives phantom DE phases; $r>1$ with $s<0$ establishes the Chaplygin gas model. The statefinder parameter for our models are

$$r = -1 - \frac{3{k_2}^2}{(2\,n+1)\,b_2 k_1 e^{\gamma_0 t}} + 2\left(-1 - \frac{3{k_2}^2}{(2\,n+1)\,b_2 k_1 e^{\gamma_0 t}}\right)^2 - \frac{9{k_2}^3\left(k_1 e^{\gamma_0 t}+k_2\right)}{(2\,n+1)^2\,{b_2}^2{k_1}^2\,(e^{\gamma_0 t})^2} \quad (25)$$

$$s = \left(-2 - \frac{3{k_2}^2}{(2\,n+1)\,b_2 k_1 e^{\gamma_0 t}} + 2\left(-1 - \frac{3{k_2}^2}{(2\,n+1)\,b_2 k_1 e^{\gamma_0 t}}\right)^2 - \frac{9{k_2}^3\left(k_1 e^{\gamma_0 t}+k_2\right)}{(2\,n+1)^2\,{b_2}^2{k_1}^2\,(e^{\gamma_0 t})^2}\right) \times \left(-4.5 - \frac{9{k_2}^2}{(2\,n+1)\,b_2 k_1 e^{\gamma_0 t}}\right)^{-1}. \quad (26)$$

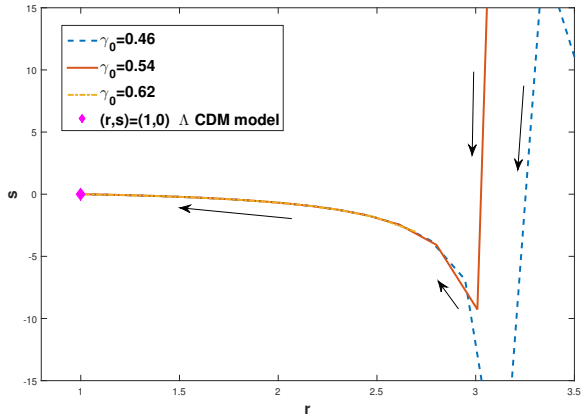

Fig. 7. Plot of statefinders for $k=-0.021$, $n=0.97$, $b_1=4.1$ and $b_2=-1.12$.

Fig. 7 illustrates the trajectory of our model in the $r-s$ plane. Notably, the behavior of $r-s$ plane closely resembles the λ_{Ras}CDM model during late times. This observation suggests that our model exhibits characteristics akin to those of dynamical DE models, such as the Chaplygin gas model ($s<0$ and $r>1$).

***r*−*q* plane** Fig. 8 shows the evolution of our model in the $r-q$ plane. Here, (r,q) variables reflect several cosmological models: $(1,-1)$ is the steady state (SS) model, while $(1,0.5)$ is the standard cold dark matter (SCDM) model. The trajectory of the λ_{Ras}CDM model follows the dotted line in Fig. 8, going from a fixed point in SCDM to a fixed position in SS. Note that our late-time model closely resembles the SS model. This trajectory in the $r-q$ plane matches DE models from the literature (Aditya et al. 2022; Singh and Kumar 2016; Naidu et al. 2018).

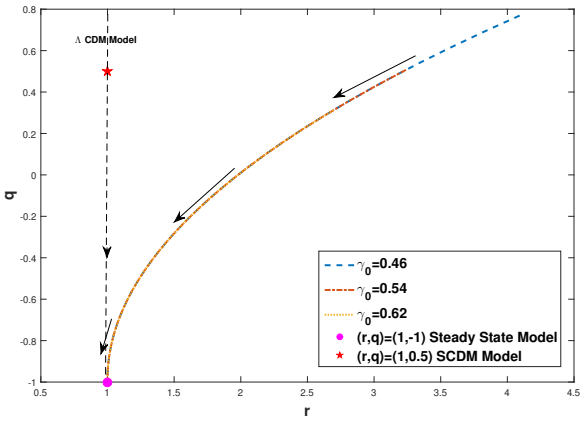

Fig. 8. Plot of the $r - q$ plane for $k = -0.021$, $n = 0.97$, $b_1 = 4.1$ and $b_2 = -1.12$.

4 Conclusions

In this study, we constructed a spatially homogeneous and anisotropic BT-*II* KHDE model within the framework of BDR theory of gravitation. By imposing physically and mathematically reasonable conditions, we derived an exact solution to the nonlinear field equations. Subsequently, we investigated various cosmological parameters to understand the behavior of our model. Our analysis led to several important conclusions:

- Our model exhibits exponential expansion throughout its evolution, with early inflation due to its extension from a finite volume. At infinite cosmic time, all physical quantities remain finite, while they tend towards infinity as cosmic time approaches zero. Additionally, the model remains homogeneous and uniform, eventually becoming isotropic and shear-free.
- The evolution of the scalar field in our KHDE model, as depicted in Fig. 1, reveals a gradual decrease over time. This declining trend mirrors the behavior observed in scalar field models of DE discussed in prior literature (Jawad et al. 2015; Naidu et al. 2020; Naidu et al. 2021; Aditya et al. 2021). As the scalar field decreases, there is a corresponding increase in kinetic energy, a characteristic feature common in such models. Additionally, the energy density of DE decreases as cosmic time t progresses. This diminishing energy density aligns with the dynamics expected in DE scenarios. However, a notable aspect of our model is the violation of the NEC, as illustrated in Fig. 2. This violation causes the Big Rip, where the universe's energy density drops with expansion, which could lead to a catastrophic event in the future. This violation supports existing observational data that the cosmos is accelerating late in time.Thus, our model demonstrates early inflation and late-time acceleration, underlining its fascinating dynamics in DE cosmology.
- The EoS parameter ω_{de} characterizes the behavior of DE in our model, showcasing a variation across quintessence and phantom regions, as depicted in Fig. 3. Moreover, the present values of the EoS parameter in our

model are in accordance with recent observations from the Planck mission, as reported by Aghanim et al. (2020) ω_{de}=$-1.56^{+0.60}_{-0.48}$ (Planck+TT+lowE), ω_{de}=$-1.58^{+0.52}_{-0.41}$ (Planck+TT, TE, EE+lowE), ω_{de}=$-1.57^{+0.50}_{-0.40}$ (Planck+TT, TE, EE + lowE + lensing),
ω_{de}=$-1.04^{+0.10}_{-0.10}$ (Planck + TT, TE, EE + lowE + lensing + BAO).

- In the $\omega_{DE} - \omega^{'}_{DE}$ plane analysis, our model demonstrates behavior consistent with the freezing region (Fig. 4), where the universe experiences notably rapid expansion. This alignment with observational evidence underscores the validity of our model's predictions regarding cosmic dynamics. Furthermore, the trajectories of the $\omega_{de} - \omega^{\prime}_{de}$ plane intersect with observational data, as reported by various studies (Ade et al. 2014; Hinshaw et al. 2018). Specifically, the values of ω_{de} and $\omega^{'}_{de}$ obtained from our model fall within the ranges provided by observations from the Planck mission, $\omega_{de} = -1.13^{+0.24}_{-0.25}$, $\omega^{\prime}_{de} < 1.32$ (Planck + WP+ BAO);
$\omega_{de} = -1.34 \pm 0.18$, $\omega^{\prime}_{de} = 0.85 \pm 0.7$ (WMAP+eCAMB+BAO+H_0). This agreement reinforces the credibility of our model's predictions and its consistency with empirical data. It is important to note that the stability analysis reveals that our KHDE model exhibits stability at initial epoch and instability at present and late-times (Fig. 5). This finding is in line with similar conclusions drawn by other researchers in the literature (Myung 2007; Jawad et al. 2013; Jawad and Chattopadhyay 2015), further emphasizing the need for additional theoretical refinement and investigation in the study of DE models.
- The smooth passage of the deceleration parameter in our model, as demonstrated in Fig. 6, indicates its capacity to precisely represent the universe's evolution from an initial decelerated phase to its present accelerated expansion. This concordance with observational evidence enhances the validity of our model in explaining cosmic dynamics. Furthermore, the agreement between the current values of the deceleration parameter q obtained from our model and those derived from observational data $q = -0.930 \pm 0.218$ $(BAO + Masers + TDSL + Pantheon + H_z)$, $q = -1.2037 \pm 0.175$ $(BAO + Masers + TDSL + Pantheon + H_0 + H_z)$, as reported by Capozziello et al. (2019), underscores the consistency and reliability of our model's predictions.
- In the last phases of cosmic history, our model follows the same behavior as the Chaplygin gas model, according to the statefinders analysis shown in Fig. 6. Also, our model seems to be moving towards a steady-state situation in the future, according to the $r - q$ plane trajectory. Notably, this trajectory bears resemblance to those observed in other DE models proposed by various researchers (Aditya et al. 2022; Singh and Kumar 2016; Naidu et al. 2018). This consistency with established DE models underscores the validity and relevance of our model's predictions within the broader context of cosmological studies.

Our model agrees well with the recent scenario of the Universe expanding at an accelerated rate, as shown by the data from recent observations. With our model, we can learn more about the anisotropic DE Universe in the context of BDR theory of gravity.

Acknowledgment: The work has been supported financially by National Board for Higher Mathematics, Department of Atomic Energy, Govt. of India under the Research project No.: 02011/8/2023 NBHM(R.P.)/R & D II/3073.

References

Abreu, E.M., et al., 2018, *EPL (Europhysics Letters), 124, 30003.*
Ade, P.A.R., et al., 2014, *Astrophys. 571, A16.*
Adhav, K.S., 2011, *Int. J. Astron. Astrophys. 1, 204.*
Adhav, K.S., et al., 2011, *Int. J. Theor. Phys. 50, 339.*
Aditya, Y., 2024, *Bulgarian Astronomical Journal, 40, 95.*
Aditya, Y., Divya Prasanthi, U.Y., 2023, *Bulgarian Astronomical Journal, 38, 52.*
Aditya, Y., et al., 2019a, *Astrophys Space Sci. 364, 190.*
Aditya, Y., et al., 2019b, *Eur. Phys. J. C 79, 1020.*
Aditya, Y., et al., 2020, *Indian Journal of Phys. 95, 383.*
Aditya, Y., et al., 2021, *New Astronomy 84, 101504.*
Aditya, Y., et al., 2022, *Int. J. Mod. Phys. A, 37(16), 2250107.*
Aditya, Y., et al., 2024, *East European Journal of Physics, 1, 85.*
Aditya, Y., Reddy, D.R.K., 2018a, *Astrophys Space Sci. 363, 207.*
Aditya, Y., Reddy, D.R.K., 2018b, *Eur. Phys. J. C, 78, 619.*
Aghanim, N., et al., 2020, *[Plancks Collaboration] A&A 641, A6.*
Akarsu, O., et al., 2020, *Eur. Phys. J. C 80, 1050.*
Akarsu, O., Kilinc, C.B., 2010, *Gen. Relativ. Gravit. 42, 119.*
Bamba, K., et al., 2018, *Eur. Phys. J. C 78, 986.*
Bekenstein, J.D., 2004, *Phys. Rev. D 70, 083509.*
Bhattacharjee, S., 2020, *Astrophys Space Sci 365, 103.*
Bondi, H., Gold, T., 1948, *Mon. Not. R. Astron. Soc. 108, 252.*
Brans, C., Dicke, R.H., 1961, *Phys. Rev. 124, 925.*
Caldwell, R., and Linder, E.V., 2005, *Phys. Rev. Lett. 95, 141301.*
Capozziello, et al., 2019, *MNRAS 484, 4484.*
Capozziello, S., De Laurentis, M., 2011, *Physics Reports 509, 167.*
Carames, T.R.P., et al., 2014, *Eur. Phys. J. C 74, 3145.*
Chunlen, S., Rangdee, P., 2021, *Phayao Research Conference 10, 2413.*
Cohen, A., et al., 1999, *Phys. Rev. Lett. 82, 4971.*
Collins, C.B., et al., 1980, *Gen. Relativ. Gravit. 12, 805.*
Copeland, E.J., et al., 2006, *Int. J. Mod. Phys. D 15, 1753.*
Darabi, F., et al., 2018, *Eur. Phys. J. C 78, 25.*
Darabi, F., et al., 2018, *Eur. Phys. J. Plus 133, 249.*
Das, D., et al., 2018, *Eur. Phys. J. C 78, 810.*
Divya Prasanthi, U.Y., Aditya, Y., 2020, *Results Phys 17, 103101.*
Divya Prasanthi, U.Y., Aditya, Y., 2021, *Phys. Dark Univ. 31, 100782.*
Drepanou, N., et al., 2022, *ur. Phys. J. C, 82, 449.*
Ghaffari, S., et al., 2020, *arXiv:2002.04972.*
Harko, T., et al., 2011, *Phys. Rev. D 84, 024020.*
Hinshaw, G.F., et al., 2018, *Astrophys. J. Suppl. 208, 19.*
Hoyle, F., 1948, *Mon. Not. R. Astron. Soc. 108, 372.*
Iqbal, A., Jawad, A., 2019, *Physics of the Dark Universe 26, 100349.*
Jahromi, A.S., et al., 2018, *Phys. Lett. B 780, 21.*
Jawad, A., Chattopadhyay, S., 2015, *Astrophys Space Sci 357, 37.*
Jawad, A., et al., 2013, *Astrophys Space Sci 344, 489.*
Jawad, A., et al., 2015 *Commun. Theor.Phys. 64, 590.*
Jawad, A., Sultan, A.M., 2021, *Adv. High Energy Phys. 2021, 5519028.*
Johri, V.B., Desikan, K., 1994, *Gen Relat Gravit 26, 1217.*
Johri, V.B., Sudharsan, R., 1989, *Australian Journal of Physics 42(2), 215.*
Kaniadakis, G., 2001, *Physica A: Stat. Mech. and its Appl. 296(3-4), 405.*
Kantowski, R., Sachs, R.K., 1966, *J. Math. Phys. 7, 433.*
Kristian, J., Sachs, R.K., 1966, *Astrophys. J. 143, 379.*
Lin, K., Qian, W.L.,2020, *Eur. Phys. J. C 80, 561.*
Maity, S., Debnath, U., 2019, *Eur. Phys. J. Plus 134, 514.*

Masi, M., 2005, *Phys. Lett. A, 338, 217.*
Maurya, S.K., Ortiz, F.T., 2020, *Physics of the Dark Universe, 29, 100577.*
Mishra, B., Sahoo, P.K., *Astrophys. Space Sci. 352, 331.*
Moffat, J.W., 1995, *Phys. Lett. B 355, 447.*
Moradpour, H., 2016 *Physics Letters B 757, 187.*
Moradpour, H., et al., 2018, *Eur. Phys. J. C 78, 829.*
Moradpour, H., et al., 2020, *Eur. Phys. J. C, 80, 1.*
Moradpour, H., Salako, I.G., 2016, *Advances in High Energy Physics 2016, 3492796.*
Myung, Y.S., 2007, *Phys. Lett. B 652, 223.*
Naidu, K.D., et al., 2018, *Eur. Phys. J. Plus 133, 303.*
Naidu, K.D., et al., 2021, *Modern Physics Letters A 36, 2150054.*
Naidu, R.L., et al., 2020, *Astrophys Space Sci 365, 91.*
Nojiri, S., Odintsov, S.D., 2003, *Phys. Rev. D 68, 123512.*
Perlmutter, S., et al., 1999, *Astrophys. J. 517, 5.*
Pradhan, A., Amirhashchi, H., 2011, *Astrophys. Space Sci. 332, 441.*
Rao, B.G., et al., 2024, *East Eur. J. Phys. 1, 43.*
Rao, V.U.M., et al., 2015, *Prespacetime Journal, 6, 947.*
Rastall, P., 1972, *Phys. Rev. D 6, 3357.*
Rastall, P., 1976, *Can. J. Phys. 54, 66.*
Reiss, A., et al., 1998, *Astron. J. 116, 1009.*
Sadeghi, J., et al., 2022, *arXiv:2203.04375.*
Saez, D., Ballester, V.J., 1986, *Phys. Lett. A, 113, 467.*
Sahni, V., et al., 2003, *JETP Lett. 77, 201.*
Salako, I.G., et al., 2016, *International Journal of Modern Physics D 25, 1650076.*
Salako, I.G., Jawad, A., 2015, *Astrophys Space Sci 359, 46.*
Santhi, M.V., Chinnappalanaidu, T., 2022, *New Astr. 92, 101725.*
Santhi, M.V., et al., 2016a, *Astrophys Space Sci 361, 142.*
Santhi, M.V., et al., 2016b, *Can. J. Phys., 94(6), 578.*
Santhi, M.V., et al., 2017a, *Can. J. Phys. 95, 179.*
Santhi, M.V., et al., 2017b, *Can. J. Phys., 95(2), 136.*
Shabani, H., Ziaie, A.H., 2020, *EPL, 129, 20004.*
Shamir, M.F., et al., 2021, *New Astronomy 89, 101624.*
Sharif,M., Zubair, M., 2010, *Astrophys. Space Sci. 330, 399.*
Sharma, U.K., Dubey, V.Ch., 2022, *Int. J. Geom. Theories Mod. Phys. 19(1), 2250010.*
Sharma, U.K., et al., 2022, *IJMPD, 31, 2250013.*
Singh, C.P., Kumar, P., 2016, *Astrophys Space Sci. 361, 157.*
Spergel, S., et al., 2007, *Astrophys. J. 170, 377* .
Susskind, L., 1995, *J. Math. Phys. 36, 6377.*
Tang, M., et al., 2019 *arXiv:1903.01034.*
Tavayef, M., Sheykhi, A., Bamba, K., Moradpour, H., 2018, *Phys. Lett. B. 781, 195.*
Thorne, K.S., 1967, *Astrophys. J. 148, 51.*
Tsallis, C., Cirto, L.J.L., 2013, *Eur. Phys. J. C 73, 2487.*
Younas, M., et al., 2019, *Advances in High Energy Physics 2019, 1287932.*